Crystallization kinetics and phase transformation in superionic lithium metaphosphate (Li_2O–P_2O_5) glass system

2009 J. Phys.: Condens. Matter 21 115102

(http://iopscience.iop.org/0953-8984/21/11/115102)

J. Phys.: Condens. Matter **21** (2009) 115102 (10pp) doi:10.1088/0953-8984/21/11/115102

Crystallization kinetics and phase transformation in superionic lithium metaphosphate (Li_2O–P_2O_5) glass system

Benson K Money and K Hariharan

Solid State Ionics Laboratory, Department of Physics, Indian Institute of Technology Madras, Chennai 600036, India

E-mail: haran@iitm.ac.in

Received 30 June 2008, in final form 18 December 2008
Published 2 February 2009
Online at stacks.iop.org/JPhysCM/21/115102

Abstract

The ionic conductivity of mol% $50Li_2O$–$50P_2O_5$ melt quenched glass shows an anomalous increase after its glass transition temperature (T_g) around 590 K. On further increasing the temperature gradually, the conductivity decreases owing to the devitrification of Li_2O–P_2O_5 glass. The evolution of devitrified crystallites was evidenced by XRD patterns. To understand the devitrification process, isothermal and non-isothermal DSC studies have been carried out on mol% $50Li_2O$–$50P_2O_5$ glass. T_g as well as T_c values are found to increase monotonically with increasing heating rates. Variation of T_g as a function of heating rates has been investigated to evaluate the lower limiting temperature of T_g and the activation energy for structural relaxation. Results of the DSC studies indicate (i) single-stage bulk crystallization of the glass, with DSC traces exhibiting a single amorphous $\Rightarrow$ crystalline (T_c) transition, (ii) an order parameter (Avrami constant) of 2.8 ± 0.1, suggesting internal (bulk) crystallization of the glass, (iii) an activation energy for crystallization equal to 121.7 kJ mol^{-1} and (iv) the activation energy for structural relaxation, E_g, to be 558.8 kJ mol^{-1}. The crystallization mechanism is closely associated with the JMA model and the experimental dataset have been fitted to a non-isothermal Avrami expression and the obtained parameters confirm the experimental results.

(Some figures in this article are in colour only in the electronic version)

1. Introduction

Several lithium ion conducting systems, investigated as glassy electrolytes, exhibit good conduction characteristics [1]. Li^+ ion conducting phosphate glasses are hygroscopic and of relatively poor chemical durability. However the addition of oxides such as PbO, Al_2O_3, TiO_2, GeO_2 and B_2O_3 makes the glasses chemically stable [2–4]. However, the metastable state of the glass tends to devitrify to an ordered stable crystalline phase, around the crystallization temperature, T_c, due to favorable thermodynamics and kinetic conditions for crystal growth in a reasonable time scale. Below T_g, crystallization is rarely observed since the kinetics of molecular dynamics are very low for the process. Thus, most of the conductivity studies of ionic glasses have been carried out below the glass transition temperature, T_g. However, conductivity studies between T_g and the crystallization temperature, T_c, could throw light on the devitrification behavior of glasses. The model glass taken up for investigation, mol% $50Li_2O$–$50P_2O_5$, exhibits a conductivity which is four orders higher than its crystalline counterpart, lithium metaphosphate, $LiPO_3$ [5]. In this context, the conductivity of mol% $50Li_2O$–$50P_2O_5$ glass has been investigated between T_g and T_c. Few systems exhibit an anomalous conductivity behavior above their T_g, owing to the phase transition or nucleation of nanocrystalline phases in the glassy matrix via controlled devitrification [6]. In fact, such controlled heat treatment can result in the amorphous to quasi-crystalline transformation of glasses, *via* surface or internal crystallization mechanisms, with strongly enhanced desired physical properties for various scientific as well as technological applications [7, 8]. However, these mechanisms are strongly dependent on the particle

size of the amorphous systems [9, 10]. The investigation of the temperature-dependent kinetics of crystal growth and nucleation mechanism provides information with respect to the stability of the glass against devitrification. In this regard, thermo analytical techniques like DTA and DSC are very powerful tools, allowing the study of such crystallization processes. Classical studies of glass crystallization usually involve laborious isothermal experiments. Hence, non-isothermal experiments are preferred, for generating kinetic data quickly with minimum number of measurements in a wide operational temperature range. The present work is directed towards conductivity studies of lithium metaphosphate bulk glass samples, mol% $50Li_2O$–$50P_2O_5$, between T_g and T_c, as well as isothermal and non-isothermal DSC studies to evaluate the thermal kinetic parameters of the devitrification process.

2. Experimental details

Lithium metaphosphate glass was prepared by a melt quenching technique. The starting materials Li_2CO_3 (lithium carbonate) and $NH_4H_2PO_4$ (ammonium dihydrogen phosphate) were weighed proportionally according to a mol% $50Li_2O$–$50P_2O_5$ composition, mixed and ground. The mixture was taken in a platinum crucible and melted at 1220 K for 1 h, with occasional stirring, in order to obtain a homogeneous melt. The bubble free clear melt was quenched between preheated copper plates in order to obtain colorless, transparent mol% $50Li_2O$–$50P_2O_5$ glass. When the same melt was slowly furnace cooled from 1220 K to room temperature, crystalline $LiPO_3$ was obtained.

Conductivity measurements, on bulk samples, as a function of temperature were performed using a Keithley 3330 Impedance Analyzer in the frequency range 40 Hz–100 KHz.

X-ray diffraction analysis was carried out by means of a diffractometer (PANalytical X'Pert PRO), using Cu Kα radiation of wavelength 1.5418 Å. Continuous XRD patterns were taken by measuring 2θ from 10° to 70°, with a step size of 0.01° and a scan step time of 5 s.

To analyze the thermo dynamical parameters, such as glass transition temperature (T_g) and crystallization temperature (T_c), isothermal and non-isothermal experiments were performed on DSC 200 PC, PHOX, NETZSCH, with bulk glass samples encapsulated in aluminum pans, in a dry N_2 atmosphere.

In the isothermal studies, the glass samples initially at temperatures below T_g, were quickly brought to the desired temperature, T_i, by a faster heating rate, for isothermal crystallization.

Non-isothermal curves were obtained with selected heating rates (3–20 K min^{-1}) in the temperature range 300–820 K. The morphology of the devitrified glasses was investigated using a Zeiss optical microscope (AXIOSKOP 2), with a magnification power of 20×.

3. Result and discussion

Figure 1 shows the x-ray diffractogram and DSC spectra (inset) of the quenched Li_2O–P_2O_5 glass.

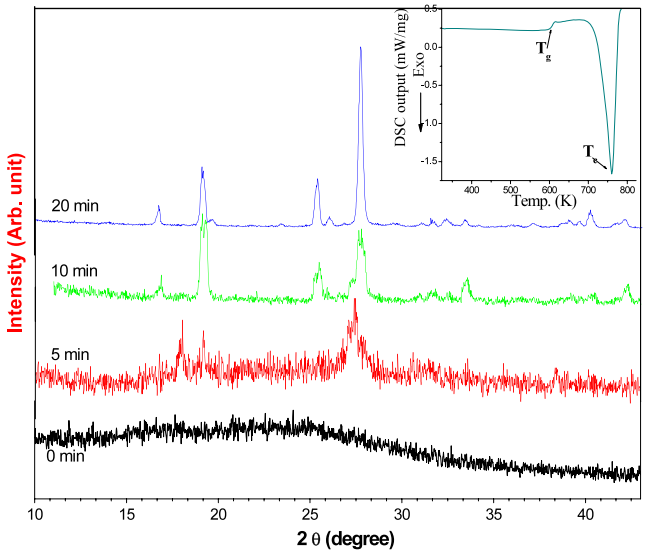

Figure 1. Evolution of Bragg peaks in the isothermally annealed (∼700 K) Li_2O–P_2O_5 glass and (inset) DSC spectrum of Li_2O–P_2O_5 glass (heating rate = 20 K min^{-1}).

The XRD pattern exhibits an absence of any Bragg peaks, indicating an amorphous nature. The DSC spectrum, recorded at a typical heating rate of 20 K min^{-1}, shows a glass transition temperature (T_g) at 604 K and crystallization temperature (T_c) at 762 K. On isothermal annealing of the glass sample above its T_g i.e. at ∼700 K, the XRD pattern displays evolution of the main Bragg peaks of $LiPO_3$, lithium metaphosphate, (figure 1). The average crystallite size of the devitrified end product was found to be ∼35 nm, as calculated by Scherer's formula. The phase transition (devitrification) can be observed directly from the crystallization microstructure through the optical micrograph shown in figure 2. As seen in the micrograph, the (a) bulk glass, Li_2O–P_2O_5 goes through the (b) glass–crystal composite phase to the final (c) glass-ceramic phase, $LiPO_3$.

In order to understand this effect of amorphous ⇒ crystalline transformations and accompanying disorder–order process on the conduction characteristics, the ionic conductivity has been investigated as a function of temperature between T_g and T_c. Figure 3 shows the temperature variation of conductivity of Li_2O–P_2O_5 glass, exhibiting an Arrhenius behavior below T_g. However, above T_g, conductivity increases anomalously (as shown in the inset). The typical conductivity value of the glass is 4.5×10^{-4} S cm^{-1} at 553 K. After several hours of annealing, the conductivity value goes down by 4 orders of magnitude to a value 4.2×10^{-8} S cm^{-1} (at 553 K) due to the conversion of glass to glass ceramic $LiPO_3$. The anomalous increase in conductivity could be attributed to the formation of a highly defective, and therefore ionically conductive, interfacial region between the glassy matrix and devitrified crystalline grain [11, 12]. A considerable decrease of the conductivity at higher temperatures is correlated with the massive crystallization of Li_2O–P_2O_5 glass. The devitrified product, $LiPO_3$ has been characterized as a monoclinic system with a unit cell of dimensions $a = 16.45$ Å, $b = 5.405$ Å, $c = 13.806$ Å and $\beta = 98.99°$, which is in agreement with the reported value for crystalline $LiPO_3$ [13]. Isothermal as well as

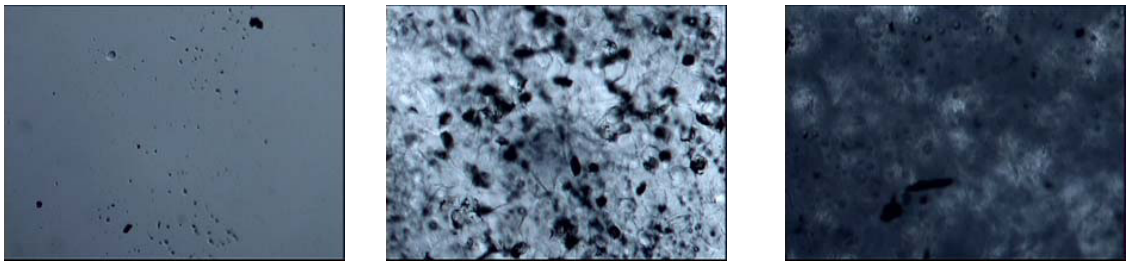

Figure 2. Optical micrographs of (a) Li_2O–P_2O_5 glass, (b) glass–crystal composite and (c) $LiPO_3$ glass ceramic.

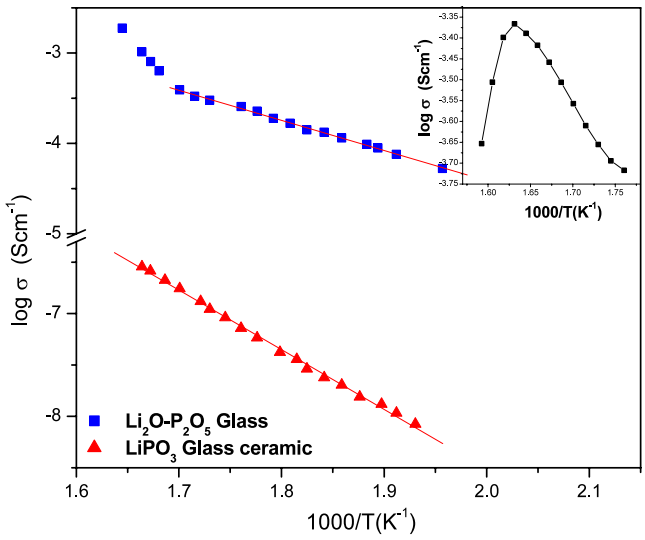

Figure 3. Arrhenius plot of Li_2O–P_2O_5 glass and its devitrified product, $LiPO_3$ glass ceramic. Inset: the increase and drop in conductivity during the devitrification process.

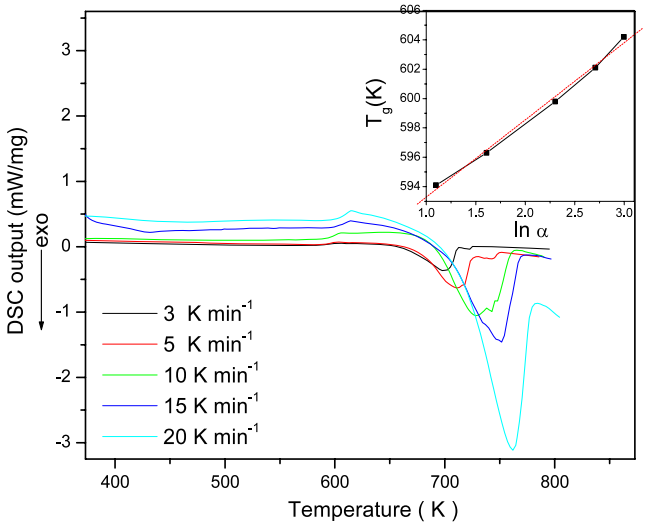

Figure 4. DSC plots of Li_2O–P_2O_5 glass for different heating rates. Inset: variation of T_g with the heating rate.

non-isothermal DSC studies, with various heating rates of 3, 5, 10, 15 and 20 K min^{-1}, have been carried out to evaluate the kinetics parameters of Li_2O–P_2O_5 glass crystallization.

3.1. Thermal analysis: Glass transition temperature

All the non-isothermal DSC traces (figure 4) exhibited the endothermic characteristics of a glass transition followed by exothermic crystallization peaks at higher temperature. The glass transition temperature, T_g and crystallization temperature, T_c for different heating rates, α are listed in table 1. The table reveals that T_g and T_c values are shifted to higher temperature with increasing heating rates [14]. The inset of figure 4 shows the variation of the glass transition temperature, T_g, as a function of heating rate, α. The plot has been linearly fitted in accordance with the empirical relation [15],

$$T_g = A + B \ln \alpha \tag{1}$$

where A and B are the empirical constants. The function T_g ($\ln \alpha$) may be nonlinear for an extended range of data. However, extrapolating the data to $\alpha = 1$ K min^{-1}, it is possible to obtain a tentative value $A = T_g^o$, which may be the lower limit of T_g. The constant B indicates the response of the configurational changes within the glass transition region to the heating rate. The steeper the slope B, the farther is the initial glassy state removed from the equilibrium state. The values of A and B are 588 K and 5.3 K respectively, for the present glass.

Table 1. DSC thermal parameters obtained from bulk mol% $50Li_2O$–$50P_2O_5$ glass.

α (K min^{-1})	T_g (K)	T_c (K)
3	594.1	697.7
5	596.3	711.4
10	599.8	729.8
15	602.1	751.4
20	604.2	762.3

Considering a possible lower limit for the glass transition temperature T_g^o, the dependence of T_g on the heating rate has been evaluated in terms of Vogel–Fulcher–Tamman (VFT) equation [16]:

$$\alpha = P \exp\left[-\frac{Q}{T_g - T_g^o}\right] \Rightarrow \ln \alpha = \ln P - \frac{Q}{T_g - T_g^o} \tag{2}$$

where T_g^o is the asymptotic value of T_g within the limit of an infinitesimally slow cooling and heating rate, and P has

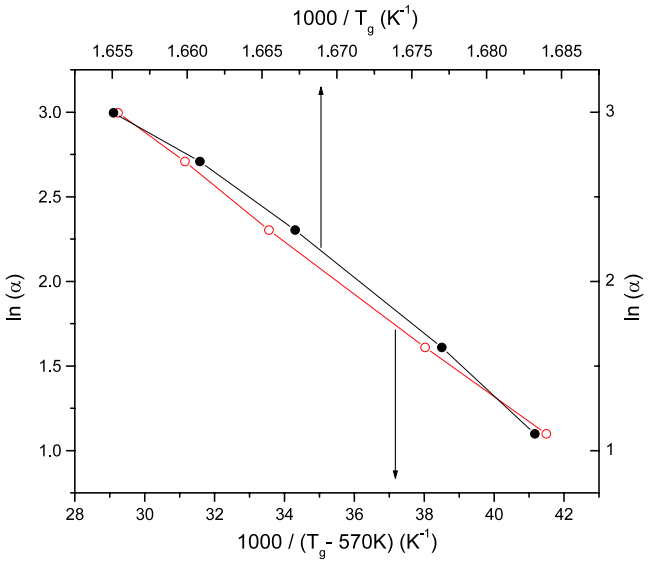

Figure 5. Plot of $\ln\alpha$ versus $1/T_g$ representing VTF fitting.

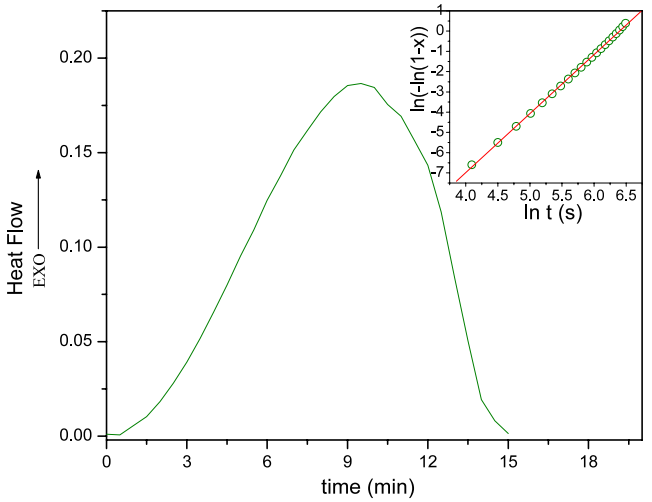

Figure 6. Isothermal crystallization peak of Li_2O–P_2O_5 glass annealed at 710 K. Inset: $\ln[-\ln(1-x)]$ versus $\ln t$ plot.

the dimension of heating rate. Figure 5 shows the best fit to the data with $T_g^o = 570$ K. Both the above formulations (equations (1) and (2)) are consistent with the assumption that there exists a temperature T_g^o which is the lower limit of T_g. The dependence of T_g on the heating rate can be satisfactorily interpreted in terms of thermal relaxation phenomena. With the increase in the heating rate, the structural relaxation time τ decreases and hence the glass transition temperature increases [14].

3.2. Crystallization kinetics

The theoretical basis for interpreting the DSC result is given by the formal theory of transformation kinetics as developed by Johnson, Mehl and Avrami [17]. In its basic form, the theory describes the evolution with time, t, of the volume fraction crystallized, x, in terms of the nucleation frequency per unit volume, I_v and the crystal growth rate, u as [17]:

$$x = 1 - \exp\left[-g\int_0^t I_v\left(\int_{t'}^t u\,\mathrm{d}\tau\right)^m \mathrm{d}t'\right] \tag{3}$$

where g is the geometric factor depending on the shape of crystal growth and m is related to the dimensionality of crystal growth.

3.3. Isothermal studies

For isothermal crystallization with a nucleation rate and growth rate independent of time, equation (3) can be simplified to the basic JMA relation as [18]:

$$x = 1 - \exp[-(kt)^n] \tag{4}$$

where, n is the Avrami constant or order parameter, related to the morphology of crystal growth and k is the overall effective reaction rate, given by

$$k = k_o \mathrm{e}^{-E/RT} \tag{5}$$

where E is the overall effective activation energy for the crystallization process. The logarithm of equation (4) gives,

$$\ln[-\ln(1-x)] = n\ln k + n\ln t. \tag{6}$$

The Avrami constant n can be evaluated at a given temperature from the isothermal DSC scan via equation (6) from the slope of $\ln[-\ln(1-x)]$ versus $\ln t$ plot. For the above isothermal studies, the glass samples were rapidly heated to different temperatures above T_g for crystal growth and held until the resulting exotherm evolved. Figure 6 shows one such exotherm for which the glass sample was rapidly heated to a temperature of 710 K, at the rate of 96 K min^{-1}. The volume fraction, x, at any time t, is given as the ratio of the partial area under the crystallization exothermic peak, which is the heat release measured at that particular time, to the total area of exothermic peak or total enthalpy of crystallization. The $\ln[-\ln(1-x)]$ versus $\ln t$ plot (inset) is quite linear and the value of n was found to be 2.9 ± 0.1.

3.4. Non-isothermal studies

Though equation (9) strictly applies only to isothermal experiments, nevertheless, it has been extensively used to derive expressions describing non-isothermal crystallization. The dependence of thermal parameters, i.e. glass transition temperatures (T_g) and crystallization temperatures (T_c) on different heating rates, α, forms the basis for the calculation of various devitrification parameters through non-isothermal processes. If T is temperature at any instant t for a particular heating rate, α, then:

$$T = T_o + \alpha t, \tag{7}$$

where T_o is the initial temperature.

Combining equations (4) and (7), the JMA equation becomes:

$$x = 1 - \exp\left[-\left(k\frac{T-T_o}{\alpha}\right)^n\right]. \tag{8}$$

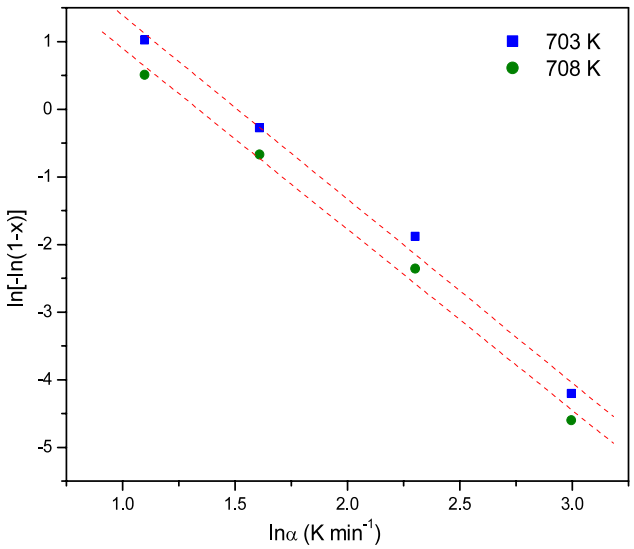

Figure 7. Plot to evaluate the Avrami constant, n, from the non-isothermal DSC.

A plot representing the above expression is shown in figure 7, where $\ln[-\ln(1-x)]$ is plotted against $\ln\alpha$ at fixed temperatures, taken at different heating rates and volume fraction, x is obtained at the same temperatures from various crystallization exotherm. The value of n is found to be 2.6 ± 0.1, which is close to the value of n evaluated by the isothermal JMA equation (6).

However, it has been well understood that for the non-isothermal case, the reaction rate, k, has a time dependence, hence equation (4) can be written as:

$$x = 1 - \exp\left[-\int_0^t k(t)\,\mathrm{d}t\right]^n. \tag{9}$$

Comparing equations (3) and (4), k^n is proportional to $I_v u^m$. In general, the temperature dependence of the nucleation frequency, I_v, and crystal growth rate, u, are not Arrhenian when a broad range of temperature is considered. However, over a sufficiently limited range of temperature both I_v and u may be approximated as:

$$I_v \approx I_{vo}\exp(-E_\mathrm{N}/RT) \tag{10}$$

$$u \approx u_o \exp(-E_\mathrm{g}/RT) \tag{11}$$

where E_N and E_g are the activation energies for nucleation and growth respectively. Hence, the overall activation energy can be expressed as, $E \approx (E_\mathrm{N} + mE_\mathrm{g})/n$. If the nucleation frequency is negligible, then, $E = mE_\mathrm{g}/n$. Equation (9) can be written as:

$$x = 1 - \exp\left(-\int_0^t \left(g' I_v u_o^m\right)^{\frac{1}{n}} \mathrm{e}^{-mE_\mathrm{g}/nRT}\,\mathrm{d}t\right)^n. \tag{12}$$

Taking the logarithm and substituting $T = T_o + \alpha t$ in the above equation

$$-\ln(1-x) = \left(\frac{(g' I_{vo} u_o^m)^{\frac{1}{n}}}{\alpha}\int_{T_o}^{T} \mathrm{e}^{-mE_\mathrm{g}/nRT}\,\mathrm{d}T\right)^n \tag{13}$$

$$-\ln(1-x) = \left(\frac{k_o}{\alpha}\right)^n \left(\int_{T_o}^{T} \mathrm{e}^{-mE_\mathrm{g}/nRT}\,\mathrm{d}T\right)^n. \tag{14}$$

Substituting, $x = mE_\mathrm{g}/nRT$ in the above integral, we get

$$\left(\int_{T_o}^{T} \mathrm{e}^{-mE_\mathrm{g}/nRT}\,\mathrm{d}T\right) = -\frac{nE_\mathrm{g}}{mR}\int_{x_o}^{x}\left(\frac{\mathrm{e}^{-x}}{x^2}\right)\mathrm{d}x \approx \frac{nE_\mathrm{g}}{mR}p(x) \tag{15}$$

where, $p(x)$ is Doyle's p-function. Combining equations (14) and (15), with a closer approximation of Doyle's p-function [19, 20], we get;

$$-\ln(1-x) = k_1\left(\frac{1}{\alpha}\right)^n\left[\frac{nE_\mathrm{g}}{mR}\mathrm{e}^{-1.052\frac{mE_\mathrm{g}}{nRT}}\right]^n. \tag{16}$$

Simplifying the above equation further, we get

$$-\ln(1-x) = k_2\alpha^{-n}\left(\mathrm{e}^{-1.052\frac{mE_\mathrm{g}}{RT}}\right). \tag{17}$$

This relation has been employed to extract the effective activation energy mE_g from the analysis of the crystallization peaks of Li_2O–P_2O_5 glass.

3.4.1. Single curve analysis. An alternate method was also employed to calculate the activation energy by the analysis of a single DSC curve. Differentiating equation (17), we get

$$\frac{1}{1-x}\frac{\mathrm{d}x}{\mathrm{d}t} = k_2\alpha^{-n}\mathrm{e}^{-1.052\frac{mE_\mathrm{g}}{RT}}1.052\frac{mE_\mathrm{g}}{RT^2}\left(\frac{\mathrm{d}T}{\mathrm{d}t}\right) \tag{18}$$

or,

$$\frac{\mathrm{d}x}{\mathrm{d}t} = k_3\alpha^{-(n-1)}\mathrm{e}^{-1.052\frac{mE_\mathrm{g}}{RT}}(1-x). \tag{19}$$

For DSC, using the relation derived by Piloyan *et al* [21], one can assume $(\mathrm{d}x/\mathrm{d}t) \propto \Delta H$, where ΔH is the enthalpy difference measured from the baseline to the crystallization DSC curve at a particular temperature T, for a single heating rate. Hence,

$$\ln\Delta H = -1.052\frac{mE_\mathrm{g}}{RT} + \ln[k_3\alpha^{-(n-1)}(1-x)]. \tag{20}$$

For $0.25 < x < 0.5$, the change in temperature has a much larger effect on the change in ΔH compared with the change in 'x' [17], thus the above equation becomes

$$\ln\Delta H = -1.052\frac{mE_\mathrm{g}}{RT} + \mathrm{const.} \tag{21}$$

Figure 8 shows the plot of $\ln(\Delta H)$ versus $1000/T$. The effective activation energy for crystallization (mE_g) calculated for different heating rates, i.e. 3 K min^{-1}, 5 K min^{-1} and 10 K min^{-1} are found to be 334.36 kJ mol^{-1}, 340.87 kJ mol^{-1} and 345.22 kJ mol^{-1} respectively. However, in order to obtain E_g and m independently, other techniques have to be utilized.

3.4.2. Sigmoidal curve fitting. There are varieties of thermo analytical techniques for the determination of the activation energy for crystallization. The utilization of these thermo analytical techniques depends on the development of good mathematical models for analyzing the experimental dataset.

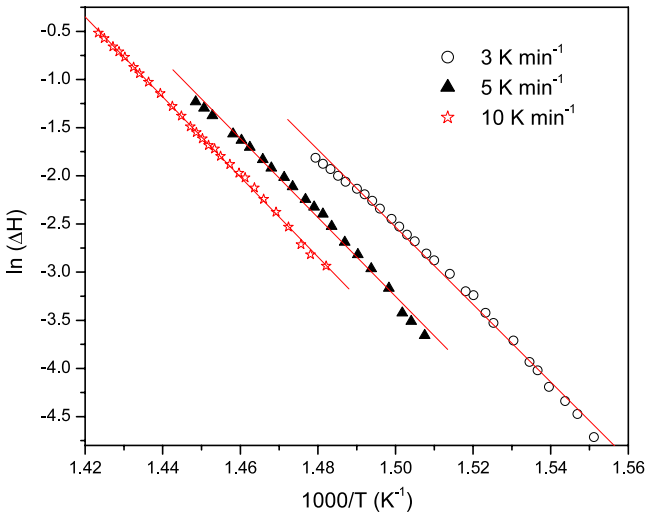

Figure 8. Piloyan plots for the crystallization of Li_2O–P_2O_5 glass at various heating rates.

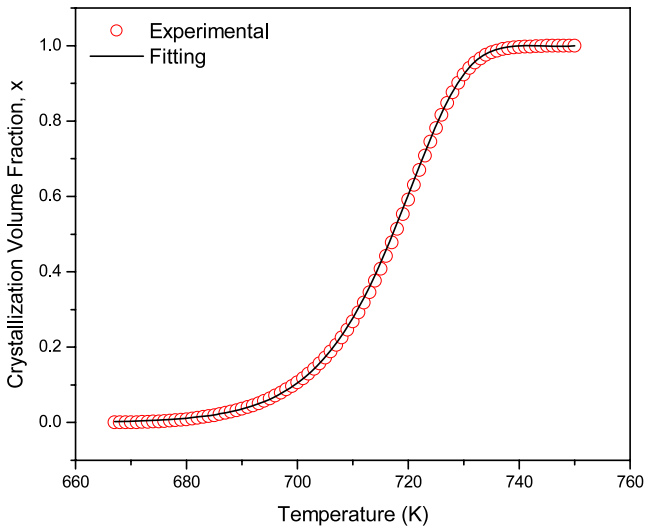

Figure 9. Sigmoidal curve showing the evolution of crystallization volume fraction, x, as a function of temperature, T, for a typical heating rate 10 K min^{-1}.

Assuming, an Arrhenian temperature dependence of nucleation frequency (equation (10)) and crystal growth rate (equation11), equation (9) becomes:

$$x = 1 - \exp\left[-gI_o u_o^m \int_0^t e^{-\frac{E_N}{RT}} \left(\int_{t'}^t e^{-\frac{E_g}{RT}} d\tau\right)^m dt'\right]. \quad (22)$$

The time-dependent isothermal JMA equation has been modified with rigorous mathematical treatment to derive a temperature-dependent expression for the volume fraction crystallized in the non-isothermal reaction, which can be well expressed as [22]

$$x = 1 - \exp\left[-Q\left(\frac{K_v T^2}{\alpha}\right)^n\right] \quad (23)$$

where, Q is a parameter, α is the uniform heating rate and K_v is the reaction rate constant with an Arrhenian temperature dependence. Assuming a constant nucleation rate, the reaction rate constant K_v is given by,

$$K_v = K_o e^{-\frac{mE_a}{nRT}}, \quad (24)$$

where $E_g(=E_a)$ is the effective activation energy of crystallization, 'n' is the Avrami exponent and 'm' is related to the mechanism of nucleation and growth. The plot of x as a function of temperature, T, for standard heating rate 10 K min^{-1}, is shown in the figure 9. It is a typical sigmoid type curve [23–25], which exhibits the bulk crystallization and excludes the chance of surface crystallization. The low temperature stage of the curve represents nucleation at various points in the sample. The intermediate stage shows the growth of nuclei, with bulk crystallization becoming dominant as the surface area of nucleation increases. The final stage shows the coalescing of all the nuclei with complete crystallization, i.e., the crystallization proceeds via nucleation and growth in Li_2O–P_2O_5 glass. The conductivity study compliments the above crystallization mechanism. Below T_g, the ionic conductivity is Arrhenius in nature. Above T_g, i.e. the initial stages of internal bulk crystallization cause the formation of $LiPO_3$ microcrystals dispersed in glass matrices. The interfacial regions between the devitrified $LiPO_3$ crystalline grain and glassy matrix leads to the formation of highly defective and therefore ionically conductive pathways, which results in an anomalous enhancement in the conductivity and a deviation from the Arrhenian nature. However, in the final stage, the conductivity falls by four orders due to massive crystallization of the glass. The observed experimental dataset of volume fraction 'x' with respect to temperature T was fitted to the above equation (23) by adjusting all the parameters. The best fit was obtained for $E_a = 121.7$ kJ mol^{-1} and $n = 3.1$. In general, when nuclei are formed in a previous heat treatment, before thermal analysis, then $n = m$, else $n \neq m$. The value of m indicates the dimensionality of crystal growth. Both the methods discussed above, utilize a single heating rate curve in order to determine the kinetic parameters of the crystallization process. The analysis of a single DSC curve recorded at a typical heating rate has its own advantages, as the multiple heating rates require the control of many parameters, such as (i) multiple baselines to be recorded and taken care of in the analysis of data, and (ii) an identical sample size is required for each heating rate. Thus, the probability of errors due to the above parameters entering the multiple scan analysis is quite high.

3.4.3. Determination of the kinetic model. The principle of reaction kinetics can be employed for thermal analysis to understand the devitrification of the glass. For this, we can assume the crystallization process as a rate of reaction given by [26],

$$\frac{dx}{dt} = k(T) f(x) \quad (25)$$

where $k(T)$ is the rate constant, represented by:

$$k(T) = k_o e^{-E_a/RT}. \quad (26)$$

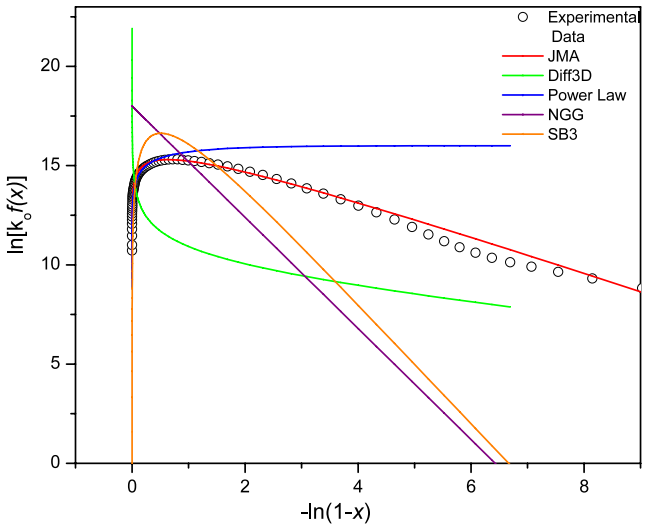

Figure 10. Plots of $\ln[k_o f(x)]$ versus $-\ln(1-x)$ for different kinetic equations as shown in table 2. Full circles correspond to experimental values of $[\ln(\mathrm{d}x/\mathrm{d}t) + E_a/RT]$ for a heating rate of 10 K min^{-1}.

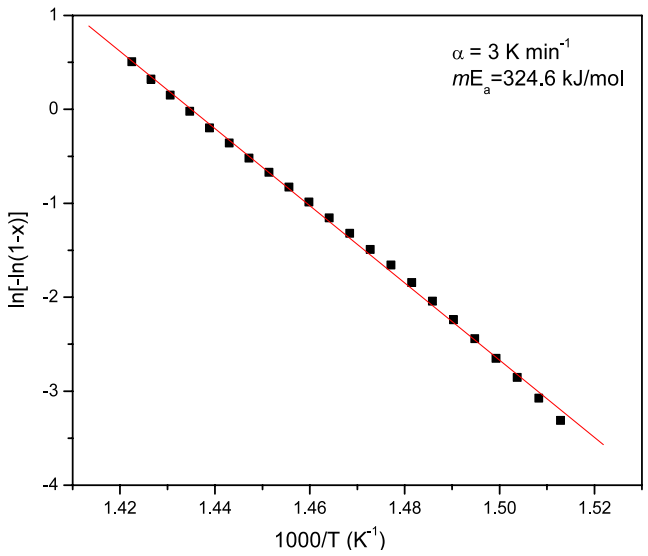

Figure 11. Plot to evaluate the effective activation energy (mE_a) for crystallization of Li_2O–P_2O_5 glass.

Table 2. Different kinetic model equations considered.

Model	$f(x)$
Johnson–Mehl–Avrami (JMA)	$n(1-x)[-\ln(1-x)]^{(n-1)/n}$
Three-dimensional diffusion (Diff3D)	$[(1-x)^{-1/3}-1]^{-1}$
Power law	$x^{(n-1)/n}$
Normal grain growth (NGG)	$(1-x)^n$
Sestak–Berggren (SB3)	$x^{n-1}(1-x)^n$

$f(x)$ is a function which reflects the mechanism of crystallization. Function $f(x)$ can be evaluated if the activation energy of crystallization, E_a, and crystallized volume fraction, x, are known. The analysis of $f(x)$ is done to distinguish which of the several kinetic models [27, 28] (table 2) can describe the crystallization process adequately.

The logarithmic form of rate reaction can be written as,

$$\ln\left(\frac{\mathrm{d}x}{\mathrm{d}t}\right) + \frac{E_a}{RT} = \ln[k_o f(x)]. \tag{27}$$

The curve fitting procedure adopted by Suriñach *et al* [29] compares plots of $[\ln(\mathrm{d}x/\mathrm{d}t) + E_a/RT]$ versus $-\ln(1-x)$ deduced from the non-isothermal thermogram, with the plots of $\ln[k_o f(x)]$ versus $-\ln(1-x)$. Figure 10 shows the plots of $[\ln(\mathrm{d}x/\mathrm{d}t) + E_a/RT]$ versus $-\ln(1-x)$ for a typical heating rate, $\alpha = 10$ K min^{-1}, with the value of E_a as the one estimated by the sigmoid curve fitting method. Using the fitting procedure for all the plots, it was found that the crystallization process for the heating rates 3 K min^{-1} $\leqslant \beta \leqslant$ 20 K min^{-1} follows the JMA model, with the JMA exponent, n, being approximately equal to 2.8.

Considering the kinetics of the nucleation and growth process involved in Li_2O–P_2O_5 glass, the JMA equation has been previously modified and represented by the equation (17). By taking the logarithm, the above equation can be written as

$$\ln[-\ln(1-x)] = -n\ln\alpha - 1.052\frac{mE_a}{RT} + \text{Const.} \tag{28}$$

This method, suggested by Matusita *et al* [30] has also been utilized to derive all the important kinetic parameters related to crystallization of Li_2O–P_2O_5 glass. This approach, however, involves multiple scans at different heating rates. The value of n, obtained by plotting $\ln[-\ln(1-x)]$ against $\ln\alpha$ at fixed temperature, was found to be 2.6 ± 0.1 (figure 7). The activation energy, mE_a, for crystallization, has been evaluated from the plot of $\ln[-\ln(1-x)]$ versus $1000/T$ for a typical heating rate of 3 K min^{-1}, as shown in figure 11. The plot was linear for the selected range of temperature. The slope gives the value of 'mE_a'. Using the value of $E_a = 121.7$ kJ mol^{-1} from sigmoid fitting plot (figure 9), the m value was calculated to be 2.7, which is almost as same as the n value. This confirms that the Li_2O–P_2O_5 glass undergoes a bulk (internal) crystallization process.

The rate of crystallization reaches its maximum at the peak crystallization temperature, T_c. Solving equation (17) for $(\mathrm{d}^2x/\mathrm{d}t^2) = 0$, the following equation is derived, which has the form of a modified Kissinger equation: [30, 31]

$$\ln\left(\frac{\alpha^n}{T_c^2}\right) = -1.052m\frac{E_a}{RT_c} + \text{const.} \tag{29}$$

A linear dependence is observed between $\ln(\alpha^n/T_c^2)$ and $1000/T_c$ as shown in figure 12 with $n = 2.6$. The slope of the plot (mE_a) is found to be 320.4 kJ mol^{-1}. Substituting $E_a = 121.7$ kJ mol^{-1} (from sigmoid curve fitting), m is found to be 2.7 implying again $m \approx n$.

The activation energy for crystallization can also be evaluated directly using the classical Kissinger method [31]:

$$\frac{\mathrm{d}\ln[\alpha/T_c^2]}{\mathrm{d}\left[\frac{1000}{T_c}\right]} = -\frac{E_{cK}}{1000R}. \tag{30}$$

From the plot of $\ln[\alpha/T_c^2]$ versus $1000/T_c$ (figure 13) the value of E_{cK} is found to be 115.7 kJ mol^{-1}. Equating E_{cK} to mE_a/n, it is again seen that $m \approx n$.

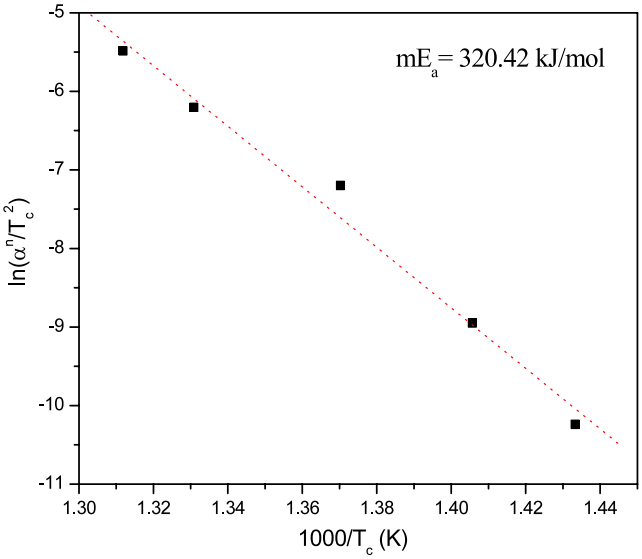

Figure 12. Plot of $\ln(\alpha^n/T_c^2)$ versus $1000/T_c$.

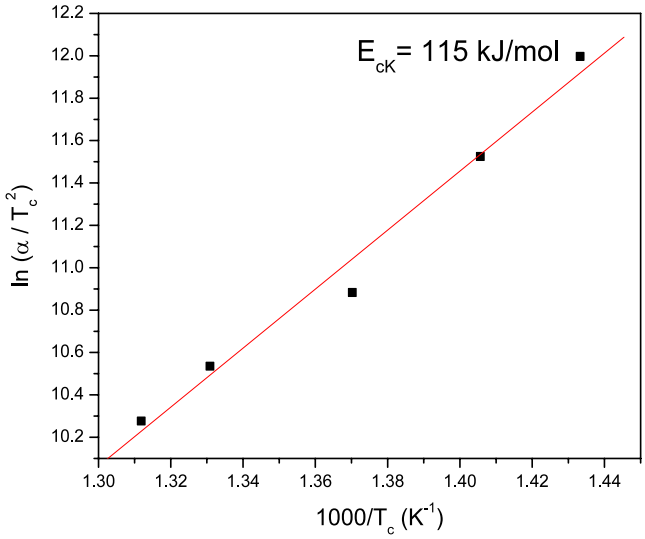

Figure 13. Kissinger plot to evaluate the activation energy for crystallization.

Equation (28) can be rearranged as:

$$\ln\alpha = -1.052\frac{m}{n}\frac{E_a}{RT} - \frac{1}{n}\ln[-\ln(1-x)] + \text{const.} \quad (31)$$

With $m = n$ and at $T = T_c$, the term is $\ln[-\ln(1-x)] \approx$ const. The above equation takes the form:

$$\ln\alpha = -1.052\frac{E_a}{RT_c} + \text{const.} \quad (32)$$

This is a modified Ozawa equation [32] and the slope of $\ln\alpha$ versus $1000/T_c$ plot, (figure 14), indicates that E_a = 128 kJ mol^{-1}.

3.5. Single-step phase transition

In order to confirm the single-step phase transformation of Li_2O–P_2O_5 glass, the isoconversional method of Flynn, Wall and Ozawa has been employed [33]. This method involves the measurement of the temperature T_x, corresponding to fixed values of the crystallized volume fraction, x, at different heating rates, α, as per the equation:

$$\ln(\alpha) = \frac{-1.052E_a(x)}{RT_x} + \text{const.} \quad (33)$$

The slope of the plot between $\ln\alpha$ and $1000/T_x$ gives the local activation energy, $E_a(x)$, as a function of the volume fraction (x) crystallized. If the determined $E_a(x)$ is the same for various values of x, the existence of a single-step reaction can be concluded with certainty. On the contrary, a change in $E_a(x)$ with increasing x is an indication of a complex reaction. In the case of Li_2O–P_2O_5, the activation energy $E_a(x)$ varied from 129.06 to 131.89 kJ mol^{-1}, which is fairly constant within the range of experimental error, thus confirming a single-step phase transformation.

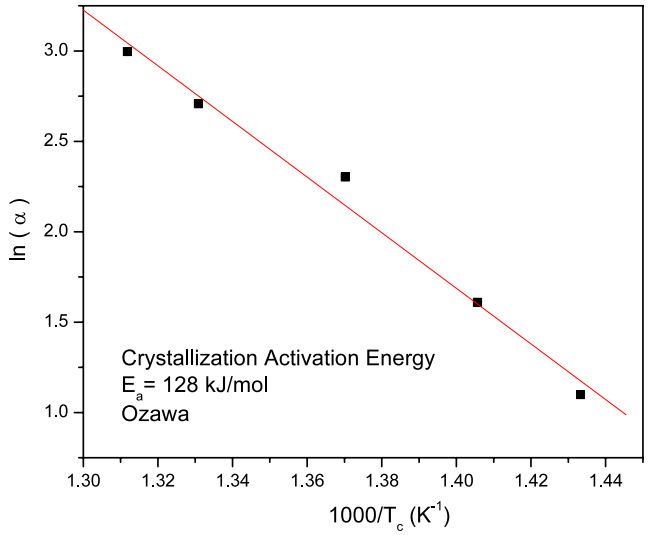

Figure 14. Ozawa plot for evaluation of crystallization activation energy.

Experimental results interpreted on the basis of different formalisms have indicated good agreement between the evaluated kinetic parameters E_a and n as shown in table 3. In general, the variations in the activation energy values derived using isothermal and various non-isothermal methods highlight the danger of assuming a crystallization mechanism for a given glass, and show that misleading results can easily be obtained if these assumptions are wrong. Glasses generally crystallize by either surface or internal (volume) crystallization. Though, both mechanisms can occur simultaneously, but in most of the systems one mechanism dominates the other. In addition, the crystallization mechanism strongly depends on the particle size, modifier concentration and varies when these factors exceed critical limits for the system. However, in any case, the final comparison of the x versus T curves, reconstructed from the set of kinetic parameters with the experimental curves, as carried out in the present study, is a good procedure for verifying the agreement between the actual behavior of the glass when it crystallizes and the theoretical

Table 3. Kinetic parameters, n and E, obtained from various methods.

Methods/parameters	nE (kJ mol^{-1})	n	E (kJ mol^{-1})
Isothermal JMA		2.9	
Non-isothermal JMA		2.6	
Single curve	345.2		
Sigmoid curve		3.1	121.7
JMA model fitting		2.8	
Matusita	324.6	2.6 ($n = m$) ($E_a = 121.7$)	
Modified Kissinger	320.4	2.7 ($E_a = 121.7$)	
Ozawa			128

model describing the crystallization reaction. Other techniques such as impedance measurements, high temperature XRD and microstructural studies can be used as complementary methods, to understand the crystallization mechanism to some extent.

3.6. Evaluation of glass transition activation energy, E_g

The glass transition temperature, T_g, exhibits a dependence on heating rate similar to that of the crystallization temperature, T_c. The activation energy for structural relaxation, E_g, is calculated using the Kissinger method [31], as per the equation

$$\ln\left(\frac{\alpha}{T_g^2}\right) = -\frac{E_g}{RT_g} + \text{const.} \tag{34}$$

The activation energy for structural relaxation, E_g, is involved in the molecular motion and rearrangement of atoms around the glass transition temperature. Figure 15 shows the plot of $\ln(\alpha/T_g^2)$ versus $1000/T_g$ for Li_2O–P_2O_5 glass. From the slope, E_g value is found to be 553.8 kJ mol^{-1}.

The Ozawa relation [32] can also be employed to calculate the glass transition activation energy as per the relation

$$\ln\alpha = -\frac{E_g}{RT_g} + \text{const.} \tag{35}$$

The E_g value evaluated from the linear plot (inset of figure 15) of $\ln\alpha$ versus $1000/T_g$ is found to be 563.8 kJ mol^{-1}. The values of the activation energy for structural relaxation, E_g, evaluated by both the methods, are in close agreement with each other. The structure of metaphosphate glasses has been shown to consist of long, entangled chains of tetrahedral phosphate structural units. Hence, it is quite possible that a high activation energy is required for the internal structural relaxation of these phosphate chains.

4. Conclusion

Deviation of the conductivity behavior from the Arrhenius nature has been observed above the glass transition temperature of the lithium metaphosphate glass during the initial stage of crystallization. However, the conductivity falls by four orders of magnitude on massive crystallization of glass to ceramic product. The variation of T_g as a function of heating rates has been investigated to evaluate the lower limiting temperature of T_g and the activation energy for structural relaxation. The crystallization kinetics of mol% $50Li_2O$–$50P_2O_5$ glass has been investigated by isothermal and non-isothermal DSC studies. The glass exhibits single crystallization exotherm corresponding to the formation of lithium metaphosphate, $LiPO_3$. The activation energies for crystallization and glass transition phenomena have been evaluated. The crystallization mechanism is closely associated with the JMA model. The experimental dataset has been fitted and the kinetic parameters obtained have been verified using various analytical techniques.

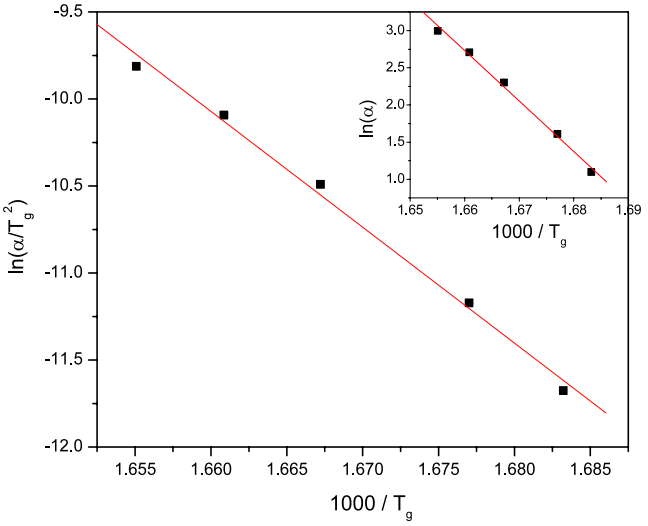

Figure 15. Plot of $\ln(\alpha/T_g^2)$ versus $1000/T_g$. Inset: plot of $\ln(\alpha)$ versus $1000/T_g$, to evaluate the glass transition activation energy.

References

[1] Tuller H L, Button D P and Uhlmann D R 1980 *J. Non-Cryst. Solids* **40** 93
[2] Abid M, Shaim A and Et-tabirou M 2001 *Mater. Res. Bull.* **36** 2453
[3] Abrahams I and Hadzifejzovic E 2000 *Solid State Ion.* **134** 249
[4] Magistris A and Chiodelli G 1985 *J. Power Sources* **14** 87
[5] Money B K and Hariharan K 2007 *Appl. Phys.* A **88** 647
[6] Adams St, Hariharan K and Maier J 1994 *Solid State Phenom.* **39/40** 285
[7] Hono K 2002 *Prog. Mater. Sci.* **47** 621
[8] Mizuno F, Hayashi A, Tadanaga K and Tatsumisago M 2005 *Electrochem. Solid State Lett.* **8** A603
[9] Ray C S, Yang Q, Huang W-h and Day D E 1996 *J. Am. Ceram. Soc.* **79** 3155
[10] Bourdin F and Rocherulle J 2004 *J. Mater. Sci.* **39** 2175
[11] Adams St, Hariharan K and Maier J 1996 *Solid State Ion.* **86–88** 503
[12] Garbarezyk J E, Jozwiak P, Wasiucionek M and Nowinski J L 2004 *Solid State Ion.* **175** 691
[13] Guitel Par J C and Tordjman I 1976 *Acta Crystallogr.* B **32** 2960
[14] Moynihan C T, Easteal A J and Wilder J 1974 *J. Phys. Chem.* **78** 2673
[15] Lasocka T M 1976 *Mater. Sci. Eng.* **23** 173
[16] Brüning R and Samwer K 1992 *Phys. Rev.* B **46** 11318
[17] Yinnon H and Uhlmann D R 1983 *J. Non-Cryst. Solids* **54** 253

[18] Avrami M 1939 *J. Chem. Phys.* **7** 1103
[19] Doyle C D 1961 *J. Appl. Polym. Sci.* **5** 285
[20] Doyle C D 1962 *J. Appl. Polym. Sci.* **6** 639
[21] Piloyan G O, Rybachikov I D and Novikova O S 1966 *Nature* **212** 1229
[22] Vasquez J, Wagner C, Villares P and Jimenez-Garay R 1996 *Acta Mater.* **44** 4807
[23] Ligero R A, Vasquez J, Casas-Ruiz M and Jimenez-Garay R 1992 *Thermochim. Acta* **197** 319
[24] Wagner C, Villares P, Vasquez J and Jimenez-Garay R 1993 *Mater. Lett.* **15** 370
[25] Popescu C 1996 *Thermochim. Acta* **285** 309
[26] Sestak J, Satava V and Wendlandt W W 1973 *Thermochim. Acta* **7** 333
[27] Malek J 1993 *Thermochim. Acta* **222** 105
[28] Atkinson H V 1988 *Acta Metall.* **36** 469
[29] Suriñach S, Baro M D, Clavaguera-Mora M T and Clavaguera N 1983 *J. Non-Cryst. Solids* **58** 209
[30] Matusita K, Komatsu T and Yokota R 1984 *J. Mater. Sci.* **19** 291
[31] Kissinger H E 1956 *J. Res. Natl Bur. Stand.* **57** 217
[32] Ozawa T 1970 *J. Therm. Anal.* **2** 301
[33] Yuan Z-Z, Chen X-D, Wang B-X and Wang Y-J 2006 *J. Alloys Compounds* **407** 163